RJ 3871 (44068) 5/13/83
Mathematics

Research Report

FREE SURFACE CALCULATION WITH APPLICATION TO DROP AND LAYER SPREADING

J. Fromm

IBM Research Laboratory
San Jose, California 95193

IBM Research Division
Yorktown Heights, New York • San Jose, California • Zurich, Switzerland

RJ 3871 (44068) 5/13/83
Mathematics

FREE SURFACE CALCULATION WITH APPLICATION TO DROP AND LAYER SPREADING

J. Fromm

IBM Research Laboratory
San Jose, California 95193

ABSTRACT: A second generation finite difference method for treating free surface problems is described. Basically, a streamfunction-vorticity formulation for incompressible flow is used, but because of the free surface, a velocity potential function is also introduced. Surface momentum equations are integrated to provide time dependent surface boundary conditions for the streamfunction and velocity potential. The numerical method is applied to spreading of liquids over no-slip surfaces and includes nonlinear behavior.

I. INTRODUCTION

In earlier work,[1,2] we developed a free surface program and applied it to the time evolution of low Reynolds number jets. The jets involved nozzle no-slip surfaces (in Ref. 2), but contact angles and their influence on meniscus behavior were sidestepped by assuming a special geometric nozzle outlet configuration. With the experience gained in this work and with interest in broader application, a more direct and accurate method has evolved. While, in the earlier programs, it was necessary to integrate the momentum equations in a complicated pattern in the interior fluid region for streamfunction surface conditions, these are now obtained at the surface itself through time dependent surface equations. Also, previously, it was necessary to solve a Poisson's equation for the pressure; now velocities and pressure may be regarded as auxiliary variables.

We shall here formulate the method in rectangular coordinates and include the axisymmetric forms in an appendix. The problem to be considered is illustrated in Fig. 1. It represents an initial configuration, somewhat difficult to realize in practice, but useful as a reference for study of layer spreading. The parameters include contact angles γ_1 and γ_2 which are both 90° in the initial configuration. They may differ after the initial instant, if the half cylinder straddles solid surfaces with differing solid-liquid interface energies. The remaining parameters are nondimensional ratios, the ratio of viscous to capillary force and the ratio of body to capillary force. The latter allows study of various orientations of the solid surface relative to gravitational acceleration, for example. Of primary interest however are spread rates in the absence of a body force. Since laboratory experiments of spreading are difficult for reasons of size and contaminated surfaces, theoretical solutions are of considerable importance.

To unify the spread rate study to be independent of size considerations, we specify a liquid area in rectangular cross section to be $A=\pi/2$, giving unit radius of curvature for the initial cylindrical configuration (Fig. 1). This then leads to expressing equilibrium solutions in terms of constant area. Such representative solutions are given in Fig. 2 with the contact angle as the adjustable parameter. Our aim is to understand the transient behavior from the initial ($\gamma_1=\gamma_2=90°$) configuration, to those equilibrium configurations determined by various γ values. For a given γ value, the ratio of viscous to capillary force gives a variety of flows ranging from similar linear behavior to oscillatory nonlinear behavior.

II. THE GOVERNING EQUATIONS

We have already mentioned the use of a scale for our problem involving an initial configuration (Fig. 1) with cross-sectional area $A=\pi/2$. This leads to a unit reference length, the radius of the half cylinder cross section,

$$r = \left(\frac{2A}{\pi}\right)^{1/2} . \tag{1}$$

For a reference velocity, we use the well-known capillary wave velocity[3]

$$v = \left(\frac{\sigma}{\rho r}\right)^{1/2} , \tag{2}$$

where σ is the surface tension coefficient and ρ is the fluid density. A time scale follows from (2), and is

$$t = \left(\frac{\rho r^3}{\sigma}\right)^{1/2} . \tag{3}$$

Through this choice of scale, we are led to the nondimensional parameters

$$\frac{W}{R} = \left(\frac{\rho v^2}{\sigma r}\right)^{1/2} \quad \text{and} \quad B = \frac{\rho r^2 a}{\sigma} . \tag{4}$$

Here ν is the kinematic viscosity of the liquid and "a" is a prespecified acceleration. W/R is a ratio of Weber number to Reynolds number and B is the Bond number. This nondimensionalization appears to be very appropriate for condensing information on drop and layer behavior.

The equations governing the interior flow are the time dependent vorticity equation

$$\frac{\partial \omega}{\partial t} + \frac{\partial u\omega}{\partial x} + \frac{\partial v\omega}{\partial y} = \frac{W}{R}\left(\frac{\partial^2 \omega}{\partial x^2} + \frac{\partial^2 \omega}{\partial y^2}\right), \tag{5}$$

and the streamfunction equation

$$\frac{\partial^2 Q}{\partial x^2} + \frac{\partial^2 Q}{\partial y^2} = -\omega . \tag{6}$$

The velocities u and v may be extracted from the streamfunction Q with

$$u = \frac{\partial Q}{\partial y} \quad \text{and} \quad v = -\frac{\partial Q}{\partial x} . \tag{7}$$

Because of the nature of the free surface boundary condition, (5) and (6) are not sufficient for solution. The problem is that the free surface streamfunction boundary condition is unknown. Our approach to this is to divide the velocities into irrotational and solenoidal parts (see Ref. 4). Thus, let

$$u = u_i + u_s = \frac{\partial \phi}{\partial x} + \frac{\partial \psi}{\partial y} \quad \text{and} \quad v = v_i + v_s = \frac{\partial \phi}{\partial y} - \frac{\partial \psi}{\partial x} . \tag{8}$$

Here ϕ is a velocity potential which satisfies

$$\frac{\partial^2 \phi}{\partial x^2} + \frac{\partial^2 \phi}{\partial y^2} = 0 , \tag{9}$$

and ψ is a secondary streamfunction which satisfies

$$\frac{\partial^2\psi}{\partial x^2} + \frac{\partial^2\psi}{\partial y^2} = -\omega \,. \tag{10}$$

The latter is distinguished from Q by having different boundary conditions. Now (5), (9), and (10) are complete for obtaining solutions, but as it turns out, it is just as convenient and more intuitive physically to use ϕ and ψ only to obtain boundary conditions for Q. It is necessary to solve (9) in the interior but not (10). The former, in a sense, replaces our need in previous work[1,2] to solve a Poisson's equation for the pressure.

To see how this comes about, first consider the local surface variables (τ, η) indicated in Fig. 1. Through rotational transformation, we have

$$u_\tau = u\cos\alpha + v\sin\alpha \quad \text{and} \quad u_\eta = -u\sin\alpha + v\cos\alpha \,, \tag{11}$$

where α is the angle of τ with x. Follow-up transformations of required equations may be done by noting that, for example,

$$\frac{\partial}{\partial x} = \frac{\partial\tau}{\partial x}\,\frac{\partial}{\partial\tau} + \frac{\partial\eta}{\partial x}\,\frac{\partial}{\partial\eta} = \cos\alpha\,\frac{\partial}{\partial\tau} - \sin\alpha\,\frac{\partial}{\partial\eta} \,. \tag{12}$$

As will be apparent later, the appropriate form of the momentum equations required at the surface follows from Lamb's[4] form of the global equations, namely

$$\begin{aligned}
&\frac{\partial u}{\partial t} + \frac{1}{2}\,\frac{\partial}{\partial x}\,(u^2+v^2) - v\omega = -\frac{\partial\left(\frac{P}{\rho}\right)}{\partial x} - \frac{W}{R}\,\frac{\partial\omega}{\partial y} + B_x \,, \\
&\frac{\partial v}{\partial t} + \frac{1}{2}\,\frac{\partial}{\partial y}\,(u^2+v^2) + u\omega = -\frac{\partial\left(\frac{P}{\rho}\right)}{\partial y} + \frac{W}{R}\,\frac{\partial\omega}{\partial x} + B_y \,.
\end{aligned} \tag{13}$$

Here use has been made of continuity

$$\frac{\partial u}{\partial x} + \frac{\partial v}{\partial y} = 0 \tag{14}$$

to write viscous diffusion in terms of vorticity and

$$\omega = \frac{\partial v}{\partial x} + \frac{\partial u}{\partial y} \tag{15}$$

has been used to obtain the given form of the nonlinear terms.

Transformations to (τ,η) frames of (13), (14) and (15) are

$$\begin{aligned}
\frac{\partial u_\tau}{\partial t} + \frac{1}{2}\ \frac{\partial}{\partial \tau}\ (u_\tau^2 + u_\eta^2) - u_\eta \omega &= -\frac{\partial\left(\frac{P}{\rho}\right)}{\partial \tau} - \frac{W}{R}\ \frac{\partial \omega}{\partial \eta} + B_\tau \\
\frac{\partial u_\eta}{\partial t} + \frac{1}{2}\ \frac{\partial}{\partial \eta}\ (u_\tau^2 + u_\eta^2) + u_\tau \omega &= -\frac{\partial\left(\frac{P}{\rho}\right)}{\partial \eta} + \frac{W}{R}\ \frac{\partial \omega}{\partial \tau} + B_\eta\ ,
\end{aligned} \tag{16}$$

$$\frac{\partial u_\eta}{\partial \eta} + u_\tau\ \frac{\partial \alpha}{\partial \eta} + \frac{\partial u_\tau}{\partial \tau} - u_\eta\ \frac{\partial \alpha}{\partial \tau} = 0\ , \tag{17}$$

$$\omega = \frac{\partial u_\eta}{\partial \tau} + u_\tau\ \frac{\partial \alpha}{\partial \tau} - \frac{\partial u_\tau}{\partial \eta} + u_\eta\ \frac{\partial \alpha}{\partial \tau}\ . \tag{18}$$

Similarly, it may be shown that the full global forms of the normal and tangential stress conditions (see Ref. 5) become

$$\text{Normal stress:}\quad \frac{P}{\rho} - \left(\frac{P}{\rho}\right)_g = -\frac{\partial \alpha}{\partial \tau} + 2\ \frac{W}{R}\ \left(\frac{\partial u_\eta}{\partial \eta} + u_\tau\ \frac{\partial \alpha}{\partial \eta}\right)\ , \tag{19}$$

$$\text{Tangential stress:}\quad \frac{\partial u_\eta}{\partial \tau} + u_\tau\ \frac{\partial \alpha}{\partial \tau} + \frac{\partial u_\tau}{\partial \eta} - u_\eta\ \frac{\partial \alpha}{\partial \eta} = 0\ . \tag{20}$$

$\left(\frac{p}{\rho}\right)_g$ in (19) is the ambient pressure in the gas (see Fig. 1); it may here be set to zero. The first term on the right of (19) is the single curvature in rectangular coordinates. It has a coefficient of unity in our chosen scaling.

With the transformed equations in hand, we proceed next by writing the surface velocities as combinations of irrotational and solenoidal parts

$$\begin{aligned} u_\tau &= u_\tau^i + u_\tau^s = \frac{\partial\phi}{\partial\tau} + \frac{\partial\psi}{\partial\eta} = \frac{\partial Q}{\partial\eta} , \\ u_\eta &= u_\eta^i + u_\eta^s = \frac{\partial\phi}{\partial\eta} - \frac{\partial\psi}{\partial\tau} = -\frac{\partial Q}{\partial\tau} . \end{aligned} \tag{22}$$

Now from (16) we are led to a double set of equations for $\dot{\phi} = \frac{\partial\phi}{\partial t}$ and $\dot{\psi} = \frac{\partial\psi}{\partial t}$. These are

$$\begin{aligned} \frac{\partial\dot{\phi}}{\partial\tau} &= -\frac{\partial\left(\frac{p}{\rho}\right)}{\partial\tau} + B_x\frac{\partial x}{\partial\tau} + B_y\frac{\partial y}{\partial\tau} - \frac{1}{2}\frac{\partial}{\partial\tau}\left(u_\tau^2 + u_\eta^2\right) , \\ \frac{\partial\dot{\psi}}{\partial\tau} &= -\frac{W}{R}\frac{\partial\omega}{\partial\tau} + u_\tau\omega , \end{aligned} \tag{23}$$

and

$$\begin{aligned} \frac{\partial\dot{\phi}}{\partial\eta} &= -\frac{\partial\left(\frac{p}{\rho}\right)}{\partial\eta} + B_x\frac{\partial x}{\partial\eta} + B_y\frac{\partial y}{\partial\eta} - \frac{1}{2}\frac{\partial}{\partial\eta}\left(u_\tau^2 + u_\eta^2\right) , \\ \frac{\partial\dot{\psi}}{\partial\eta} &= -\frac{W}{R}\frac{\partial\omega}{\partial\eta} + u_\eta\omega . \end{aligned} \tag{24}$$

Equations (24) are not usable and are included only to show the consistency of the formulation following from Lamb's form. The $u_\tau\omega$ term of the second of (23) compared to the $u_\eta\omega$ term of the second of (24) simply reflects a property of the streamfunction.

It is clear then that with (23) we may forward march $\dot{\phi}$ and $\dot{\psi}$ and hence ϕ and ψ to obtain surface boundary conditions. With these quantities in hand and with solid-liquid interface boundary conditions (to be discussed in the following), we may obtain ϕ and ψ in the interior with (9) and (10). Instead, however, we obtain only ϕ in the interior so that u_η^i may be extracted. u_η^s may be obtained directly from ψ at the surface so that with (22) we can obtain free surface boundary conditions for Q.

Solving (6) in the interior permits us to obtain u_τ at the surface and with the inverse transformation of (11), the global surface velocities u and v. Local (τ,η) reference frames are transported to new positions in a Lagrangian sense with

$$\frac{dx}{dt} = u \quad \text{and} \quad \frac{dy}{dt} = v \,. \tag{25}$$

The angles α relating the global and local frames of reference are, of course, changed at each modification of the surface by (25). The local vorticities and pressures required in (23) follow from (18) and (19). We avoid normal derivatives by using (20) in (18) and (17) in (19). Thus, the surface vorticity and pressure equations become

$$\omega = 2 \left(\frac{\partial u_\eta}{\partial \tau} + u_\tau \frac{\partial \alpha}{\partial \tau} \right) , \tag{26}$$

and

$$\frac{P}{\rho} = - \frac{\partial \alpha}{\partial \tau} - 2 \frac{W}{R} \left(\frac{\partial u_\tau}{\partial \tau} - u_\eta \frac{\partial \alpha}{\partial \tau} \right) . \tag{27}$$

Our final consideration is the no-slip boundary condition at the solid surface. Clearly we must have

$$v_b = \left(\frac{\partial \phi}{\partial y}\right)_b - \left(\frac{\partial \psi}{\partial x}\right)_b = -\left(\frac{\partial Q}{\partial x}\right)_b = 0 , \tag{28}$$

and

$$u_b = \left(\frac{\partial \phi}{\partial x}\right)_b + \left(\frac{\partial \psi}{\partial y}\right)_b = \left(\frac{\partial Q}{\partial y}\right)_b = 0 . \tag{29}$$

To satisfy the former, we require

$$\left(\frac{\partial \phi}{\partial y}\right)_b = \left(\frac{\partial \psi}{\partial x}\right)_b = 0 , \tag{30}$$

and for the latter

$$\left(\frac{\partial \psi}{\partial y}\right)_b = -\left(\frac{\partial \phi}{\partial x}\right)_b = -(u_i)_b . \tag{31}$$

While (31) is not used in calculation, it is important to see in what respect ψ and Q boundary conditions differ here. With consideration of (31), we have that

$$\omega_b = -\left(\frac{\partial^2 Q}{\partial y^2}\right)_b = -\left(\frac{\partial^2 \psi}{\partial y^2}\right)_b - \left(\frac{\partial u_i}{\partial y}\right)_b . \tag{32}$$

This is the usual "afterthought[6]" determination of the boundary vorticity at a no-slip surface that follows from (6). If we were to use ψ as a calculation variable, we would specify ψ as constant on the no-slip surface in accordance with (30), but the "afterthought" vorticity would require a contribution obtained from ϕ also. This abbreviated discussion is based on the anticipated use of lowest order difference approximations for the Laplacian which allows vorticity values to be placed at the no-slip surface as a follow-up of a single pass solution of elliptic equation (6).

III. THE FINITE DIFFERENCE EQUATIONS AND ORDER OF CALCULATION

Here we use a uniform rectangular grid for calculation of internal fields. A square grid is preferred whenever possible, because any stretching is accompanied by larger truncation errors. We regard the surface as being composed of Lagrangian particles to which are attached the local (τ,η) coordinate frames. Generally, 3 to 10 particles cover a mesh distance of the internal grid. One assumes that the accuracy is governed by the Eulerian (internal) grid, and hence the more dense surface grid is only a means of providing sufficiently adequate particles that motion does not lead to intergrid regions, vacant of associated surface grid points. This would affect the logic by which the program determines the appropriate approximations to be used near the free surface. Local interpolation of surface variable values occurs often throughout calculation in order to align information along grid lines. Where information is required for such alignment, linear interpolation is used. On the other hand, we also need to transfer information from interior points to the surface when normal derivatives at the surface are required. This involves taking one sided derivatives at nearest surface approach to selected interior points and then distributing this information to all surface particle positions. In these cases Lagrange interpolation up to fourth order is used, except near contact points (lines). It will be noted that interior flow fields are required for vital information at the surface in only two instances. One of these is to obtain u_η^i from the internal velocity potential. The other is to obtain u_τ from the final streamfunction solution.

Let us consider a case where the half cylinder fluid configuration is placed on a solid surface, Fig. 1. Motion is initiated through the input contact angles, if they differ from 90°, causing a nonuniform curvature $(\partial\alpha/\partial\tau)$ near the contact lines. This is reflected as a reduced pressure which manifests itself in a spacial change of $\dot{\phi}$, the time derivative of the

velocity potential. In the given case, we choose $\dot{\phi}$ and ϕ to be forever zero at the crest of the initial configuration (Fig. 1). Integrating both directions from this point and recognizing the conservative form of (23), we may write

$$\dot{\phi}_k = \left(\frac{P}{\rho}\right)_0 - \left(\frac{P}{\rho}\right)_k + B_x(x_k - x_0) + \frac{1}{2}\left[(u_\tau^2 + u_\eta^2)_0 - (u_\tau^2 + u_\eta^2)_k\right], \tag{33}$$

where k represents the k'th particle relative to the reference o'th particle at the initial lens crest. If the surface velocities and derivatives are stored quantities, we have

$$\left(\frac{P}{\rho}\right)_k = -\left(\frac{\partial \alpha}{\partial \tau}\right)_k + 2\,\frac{W}{R}\left[(u_\eta)_k\left(\frac{\partial \alpha}{\partial \tau}\right)_k - \left(\frac{\partial u_\eta}{\partial \tau}\right)_k\right], \tag{34}$$

where derivatives are evaluated locally by first order differences.

With a time dependent free surface boundary condition

$$\phi_k^{n+1} = \phi_k^n + \Delta t\ \dot{\phi}_k\ , \tag{35}$$

and a solid surface condition (30) in the form

$$\phi_{i,j_0-1/2} = \phi_{i,j_0+1/2}\ , \tag{36}$$

we are in a position to solve (9) in the fluid interior. Here we are using (i,j) as the (x,y) grid index ($j=j_0$ at the solid boundary), and n as an explicit time index. Note in Fig. 1 that ϕ is defined at cell centers.

We postpone discussion of (9) because the parallelism of ψ and ϕ makes combined discussion of (6) and (9) appropriate. The analogous expression to (33) for ψ is, for example,

$$\dot{\psi}_{k+1} = \dot{\psi}_k + \frac{W}{R}\ (\omega_k - \omega_{k+1}) + \frac{1}{2}\ [(u_\tau\omega)_{k+1} + (u_\tau\omega)_k](\tau_{k+1} - \tau_k) \qquad (37)$$

with

$$\psi_k^{n+1} = \psi_k^n + \Delta t\ \dot{\psi}_k\ . \qquad (38)$$

We arbitrarily take $\dot{\psi}$ and ψ to be forever zero at the solid-fluid boundary and take a mean of outward integrations from the contact lines to reduce truncation errors. Note that $\dot{\psi}$ is here treated locally because of the $u_\tau\omega$ term.

Assume that u_η^i is available to us (as it will be after solution of (9)), and we obtain u_η^s directly from ψ at the surface. Now by integrating from the contact lines (Q forever zero there), we obtain Q at the surface with

$$Q_{k+1} = Q_k + (u_\eta^i + u_\eta^s)\Delta\tau_{k+\frac{1}{2}}\ . \qquad (39)$$

With Q also zero at the entire solid-liquid interface, we may solve (6).

Now equations (6) and (9) are integrated numerically in identical form for the Laplacian, except for displacement of ϕ and Q on the discrete grid (see Fig. 1). This is true for the rectangular case, but not so for the axisymmetric case (see appendix). Here we will

discuss only Q, in terms of the forms that the difference equations take. In the case of (6), the right-hand side must be determined. The surface vorticity values follow from (26) as

$$\omega_k = 2 \left[\left(\frac{\partial u_\eta}{\partial \tau} \right)_k + (u_\tau)_k \left(\frac{\partial \alpha}{\partial \tau} \right)_k \right] . \tag{40}$$

No-slip surface vorticity follows as an afterthought to earlier solution of (6) and is given by

$$\omega_{i,j_0} = - \frac{2u_{i,j_0+1/2}}{\Delta y} , \tag{41}$$

where we agree to let $u_{j_0-1/2} = -u_{j_0+1/2}$. This is consistent with lowest order differencing of (6) and with Eq. (32) (Ref. 6).

The time dependent vorticity equation (5) provides us with interior vorticity values. It is integrated in flux form, as described in Ref. 7. Near the free boundary, vorticity values are updated if they lie greater than a half mesh distance from the surface. If less than a half mesh distance, they are not required in (6) and may take on interpolated values, partly for the sake of completing the field. Because other interior points might make use of these interpolated points, one requires that free surface data enter the difference form of (5) for those points which are greater than one but less than one and one-half mesh distances from the surface. Ultimately the "floating" or interpolated mesh values must enter into normal computation or are eliminated by the surface moving beyond them (so to speak). While it is possible with precise timing to assign more correct values to these "floating" points, we have up to now assumed their interpolated values are sufficiently accurate starting values when they become an active part of the system.

This "floating" nature of mesh points less than a half mesh distance from the surface is crucial in solutions to (6) and (9). If mesh values are not required to be floating, truncation

errors become larger and larger as the mesh point merges with the surface. Thus, by confining active mesh points to those as previously stated, the accuracy of unbalanced differences is kept to a minimum. We therefore write for a "somewhat" general difference form of (6) (see Fig. 3) the "star" formula

$$Q_0 = (a_1Q_1 + b_1Q_2 + c_1Q_3 + d_1Q_4 + \omega_0)/\left(\frac{2}{ac} + \frac{2}{bd}\right) \tag{42}$$

where

$$a_1 = \frac{2}{a(a+c)}, \quad c_1 = \frac{2}{c(a+c)},$$

$$b_1 = \frac{2}{b(b+d)}, \quad d_1 = \frac{2}{d(b+d)},$$

and

$$\frac{1}{2}\Delta x \le a \le \frac{3}{2}\Delta x, \quad \frac{1}{2}\Delta x \le c \le \frac{3}{2}\Delta x$$

$$\frac{1}{2}\Delta y \le b \le \frac{3}{2}\Delta y, \quad \frac{1}{2}\Delta y \le d \le \frac{3}{2}\Delta y.$$

Equation (42) is not, in fact, as general as we may need. When concave curvatures are very small, a special form must be devised in order to satisfy the limitations on a, b, c, or d. The same is true for very large concave curvatures, but there is no corresponding difficulty with convex surfaces. We would have no problem even with the former, if a diagonal equivalent of (42) could be used. Unfortunately the diagonal form is relevant only to a square grid, otherwise an extra grid point is required to remove the cross term from the approximation! Fortunately the "Man 1" layout of Fig. 3 is a simple modification of (42). That is, require $a=\Delta x$, then take

$$Q_1 = [\Delta y Q_5 + (b' - \Delta y) Q_8] / b' \tag{45}$$

where

$$\Delta y \leq b' \leq \frac{3}{2} \Delta y .$$

The reason for this modification is that otherwise we may have $a >> (3\Delta x/2)$, and hence have large truncation errors.

The "Man 2" formula (layout sketched in Fig. 3) is more complicated and is not included here. However the surface point "5" may be taken as the mean of adjacent values at the surface along the horizontal and vertical grid lines. The distances such as (a) and (b) may be taken, for example, as

$$a = \frac{(a' - \Delta x) + \Delta x}{2} = \frac{a'}{2} . \tag{46}$$

With these approximations, one may derive an appropriate formula.

The determination of the normal velocity u_τ has already been mentioned. Generally the range of surface particles to be tested for proximity to a given internal grid point can be restricted to a short interval because of retention of information relating key particles to grid lines. Testing on squared distances saves time and seems satisfactory in finding the closest approach particle.

Only the single particle in contact with the solid no-slip surface (at the contact line) is permitted *free* slip. This is the simplest assumption one can make and is probably as far as one can go on the basis of continuum mechanics alone. For all other particles on the free surface the global (u,v) velocities are obtained by rotational transformation, but at the

contact point the inverse transformation (Eq. 11) is required because u and v are the given quantities while u_τ and u_η are not given.

Finally the best assumption concerning curvature at contact lines seems to be an extrapolation of the input contact angle beyond contact. This gives the proper angular gradient ($\partial\alpha/\partial\tau$) and works well in approach to equilibrium in that it provides the ultimately *constant* curvature surface.

An automated addition or deletion of surface grid points is useful in maintaining as near equal interparticle spacing as possible. This keeps truncation errors down. We, of course, assume that the surface contains an infinite number of particles and we prudently select a subset of these to carry the surface information.

IV. LOGIC AND LIMITATIONS

Clearly keeping track of Eulerian grid points which belong to the active points of calculation can pose difficult programming problems. Here, we trace the surface particles in sequence and tabulate grid line crossings (whether vertical or horizontal). Knowing the direction of the outward normal to the fluid surface at the first particle is sufficient to identify the interior from the exterior for the remainder of the sequence. Several crossings of a single grid line can be troublesome. One is therefore limited to reasonably smooth variation of the surface and hence to a sensible range of the fluid parameters.

We make use of the "static" contact angle throughout. The so-called "apparent contact angle" is based on the assumption that the fluid surface is always a spherical lens, in the case of a drop (here a cylindrical lens). This is perhaps approximately true for very viscous fluids or very small drops with a negligible body force. Nevertheless the meniscus, however small, must exist to initiate fluid motion and hence must be part of a time sequence

calculation. Also, because the study is theoretical, we here first consider ideally flat and clean surfaces. There is some debate whether this infers that contact angles are static. We assume they are. The fluid particle at the no-slip surface is always positioned, relative to its neighbor, to give the input contact angle. Numerical errors are probably greatest where the curvature is locally large. This seems to be born out in that small contact angles cause the program to fail in the first few time steps from the initial configuration (Fig. 1).

On the basis of our current system of numerical algorithms, we limit the range of contact angles to $25° \leq \gamma \leq 125°$. To maintain a reasonably smooth overall surface, we restrict W/R to be greater than 0.002. This may be optimistic, but one can use a finer grid if necessary to reach these small values. We have insufficient experience regarding the range of Bond number, but it will depend upon the associated W/R value. Some smoothing of surface variable values can be done to reduce computer noise, but this must be restricted to higher derivatives, never to the streamfunction or potential function. Further, smoothing must be regarded as an expedient only in lieu of using a finer grid. Smoothing of particle positions can be justified to some extent in that small variations, not resolvable by the grid, will be removed by surface tension acting locally. Mass loss is a good limiting consequence of such practices, however.

V. RESULTS

We illustrate layer spreading with an example in which W/R=10, B=0, and $\gamma_1=\gamma_2=45°$. This is a case which is in the linear domain; the transition where nonlinearity becomes important is at W/R~0.5. This may vary somewhat with γ. Figure 4 gives a series of five successive states of time dependent spreading. In Table I, we list pertinent data for each time illustrated. Streamlines and lines of constant velocity potential define the flow. The former are solid lines with negative values including tick marks. Constant potential lines

are dashed lines with a characteristic normal trend toward the solid surface. Flow throughout the sequence is symmetrically downward toward contact lines. The flow is initially rapid and diminishes as equilibrium is approached. This is reflected in the plot intervals ΔQ of Table I which become smaller with time. Experience suggests that the surface energy minimum is broad, and hence even in a very viscous case critical damping may not occur, *i.e.*, some overshoot always seems to occur.

The velocity potential lines are included mostly to provide additional insight into the method of calculation. They do not represent the full solution as exists in the streamlines. They suggest isobars with low pressure at the contact lines but the velocity potential has its maximum there (*i.e.*, $\mathbf{u}_i=\nabla\phi$ with $\mathbf{u}_i$ and $\mathbf{u}$ similarly directed here).

The meniscus is barely visible at the earlier times, but we know that the low pressure there is immediately felt throughout the liquid in the incompressible case. The meniscus curvature diminishes with time, passes through zero curvature, and ultimately meets with the changing curvature of the surface of the bulk of the liquid. Thus, the early part of the flow is driven by the low pressure at the meniscus, but as the sign of the curvature changes, the driving pressure comes from other regions of the surface in such a way as to finally equalize the pressure throughout at a lower value than originally existed.

An interesting aspect of the flow is less apparent in this rather viscous example. That is, the effect of the no-slip surface. Only the contact line itself is allowed "free" slip in the sense that $u_b\neq 0$ there. We do not have true free slip because ω_b the vorticity at the contact line is not necessarily zero, although it can be shown that the contributions to ω (Eq. 26) tend to cancel one another. The vorticity on the solid surface of course affects the flow. Because of the relatively high viscosity, the diffusion of no-slip boundary vorticity is rapid in

this example and, even at early times, the faster fluid motion is near the free surface (a vacancy of streamlines near the solid surface). For less viscous cases, one can observe slow growth of the boundary layer, allowing obvious faster spreading at early times.

For an additional example, we include Fig. 5, a case in which W/R=0.05, B=0, $\gamma_1=45^\circ$ and $\gamma_2=30^\circ$. This simulates a situation in which surface energies differ at the contact lines. One might think of this as introducing a blotter at the edge on the right of a stationary region of fluid on a flat surface. We do, in fact, begin the calculation with equilibrium for $\gamma_1=\gamma_2=45^\circ$, but then modify γ_2 to be 30° to initiate the motion. Plot information for Fig. 5 is given in Table II. A history plot reveals that the right contact line moves into the higher surface energy region at a near constant velocity at first, while the left contact line remains stationary. Once the motion has progressed like a rarefaction wave to the left contact line, one has an exponential build up of the velocity of the layer (except for the moderating effect of the no-slip surface). Note the sparseness of streamlines at the solid surface. The late time velocity buildup is reflected in the constant plot interval of Q followed by a growing one at later times. Also, it should be noted that the "rarefaction" manifests itself in ϕ_{min} of Table II as increasingly negative values in time.

Finally, we summarize data collected from a series of calculations of spreading with $\gamma_1=\gamma_2=45^\circ$ as in our first example (Fig. 4). The equilibrium distance (ℓ) of Fig. 2 may be used as a reference for a measure of spread times with tabulated first arrival times at a distance (ℓ) of the contact line. It is found that for W/R>0.5, these nondimensional times vary as

$$t \approx 1.25 + 3\,\frac{W}{R}\,. \tag{47}$$

For $W/R < 0.5$, the spread time is surprisingly a constant function of W/R at $t \sim 1.25$. Thus, assuming water on glass (for example) takes on a 45° contact angle at equilibrium, a one millimeter drop should first reach equilibrium in about 5 milliseconds. More results of drop and layer spreading are to appear elsewhere.

APPENDIX

THE AXISYMMETRIC EQUATIONS

Constant volume ($V=2\pi/3$) equilibrium solutions for $B=0$ and $\gamma_1=\gamma_2$ may be written in the axisymmetric case in correspondence to Fig. 2 as

$$r_0^3 = \frac{2}{2 - \cos\gamma\ (\sin^2\gamma + 2)} \tag{A1}$$

where again

$$h = r_0(1 - \cos\gamma)\ , \qquad \ell = r_0 \sin\gamma\ .$$

The vorticity equation, taking u in the axial (z) direction and v in the radial (r) direction, becomes

$$\frac{\partial\omega}{\partial t} + \frac{\partial u\omega}{\partial z} + \frac{\partial v\omega}{\partial r} = \frac{W}{R}\left[\frac{\partial^2\omega}{\partial z^2} + \frac{\partial}{\partial r}\left(\frac{1}{r}\ \frac{\partial\omega r}{\partial r}\right)\right]. \tag{A2}$$

The streamfunction equation becomes

$$\frac{\partial^2 Q}{\partial z^2} + r\ \frac{\partial}{\partial r}\left(\frac{1}{r}\ \frac{\partial Q}{\partial r}\right) = -\,r\omega \tag{A3}$$

where

$$ur = \frac{\partial Q}{\partial r} \qquad \text{and} \qquad vr = -\,\frac{\partial Q}{\partial z}\ , \tag{A4}$$

and

$$\omega = \frac{\partial v}{\partial z} - \frac{\partial u}{\partial r}\ , \tag{A5}$$

and

$$\frac{\partial u}{\partial z} + \frac{1}{r} \frac{\partial vr}{\partial r} = 0 . \tag{A6}$$

If we split the velocity into irrotational and solenoidal components in the form

$$u = u_i + u_s = \frac{\partial \phi}{\partial z} + \frac{1}{r} \frac{\partial \psi}{\partial r} , \qquad v = v_i + v_s = \frac{\partial \phi}{\partial r} - \frac{1}{r} \frac{\partial \psi}{\partial z} , \tag{A7}$$

(A6) becomes

$$\frac{\partial^2 \phi}{\partial z^2} + \frac{1}{r} \frac{\partial}{\partial r} \left(r \frac{\partial \phi}{\partial r} \right) = 0 \tag{A8}$$

and the secondary streamfunction ψ satisfies (A5) in the form

$$\frac{\partial^2 \psi}{\partial z^2} + r \frac{\partial}{\partial r} \left(\frac{1}{r} \frac{\partial \psi}{\partial r} \right) = - r\omega . \tag{A9}$$

Rotational transformation to surface coordinates of Lamb's form of the global axisymmetric momentum equations gives

$$\frac{\partial u_\tau}{\partial t} + \frac{1}{2} \frac{\partial}{\partial \tau} \left(u_\tau^2 + u_\eta^2 \right) - u_\eta \omega = - \frac{\partial \left(\frac{p}{\rho} \right)}{\partial \tau} - \frac{W}{R} \left(\frac{1}{r} \frac{\partial \omega r}{\partial \eta} \right) + B_z \frac{\partial z}{\partial \tau} \tag{A10}$$

$$\frac{\partial u_\eta}{\partial t} + \frac{1}{2} \frac{\partial}{\partial \eta} \left(u_\tau^2 + u_\eta^2 \right) + u_\tau \omega = - \frac{\partial \left(\frac{p}{\rho} \right)}{\partial \eta} + \frac{W}{R} \left(\frac{1}{r} \frac{\partial \omega r}{\partial \tau} \right) + B_z \frac{\partial z}{\partial \eta} . \tag{A11}$$

Note that only a z component of B is indicated here for brevity.

The separation of local velocity components at the surface into rotational and solenoidal parts follows from (A7) so that

$$u_\tau = u_\tau^i + u_\tau^s = \frac{\partial \phi}{\partial \tau} + \frac{1}{r} \frac{\partial \psi}{\partial \eta}, \qquad u_\eta = u_\eta^i + u_\eta^s = \frac{\partial \phi}{\partial \eta} - \frac{1}{r} \frac{\partial \psi}{\partial \tau}, \tag{A12}$$

and

$$\begin{aligned} u_\tau &= \frac{1}{r} \frac{\partial Q}{\partial \eta} \\ u_\eta &= -\frac{1}{r} \frac{\partial Q}{\partial \tau} \end{aligned} \tag{A13}$$

Again taking $\dot{\phi} = \frac{\partial \phi}{\partial t}$ and $\dot{\psi} = \frac{\partial \psi}{\partial t}$, Eqs. (A10) and (A11) may be written

$$\frac{\partial \dot{\phi}}{\partial \tau} = -\frac{\partial \left(\frac{p}{\rho}\right)}{\partial \tau} + B_z \frac{\partial z}{\partial \tau} - \frac{\partial}{\partial \tau} \left(u_\tau^2 + u_\eta^2\right) \tag{A14}$$

$$\frac{\partial \dot{\psi}}{\partial \tau} = -\frac{W}{R} \frac{\partial \omega r}{\partial \tau} + u_\tau \omega r \tag{A15}$$

$$\frac{\partial \dot{\phi}}{\partial \eta} = -\frac{\partial \left(\frac{p}{\rho}\right)}{\partial \eta} + B_z \frac{\partial z}{\partial \eta} - \frac{\partial}{\partial \eta} \left(u_\tau^2 + u_\eta^2\right) \tag{A16}$$

$$\frac{\partial \dot{\psi}}{\partial \eta} = -\frac{W}{R} \frac{\partial \omega r}{\partial \eta} + u_\eta \omega r . \tag{A17}$$

The tangential stress and vorticity (20) and (26) remain the same as for the rectangular case, but the normal stress condition is modified by an additional curvature and by the presence of r in the continuity equation. Thus, (19) becomes

$$\frac{P}{\rho} = \left(\frac{\cos\alpha}{r} - \frac{\partial \alpha}{\partial \tau}\right) - 2 \frac{W}{R} \left(\frac{\partial u_\tau}{\partial \tau} + \frac{v}{r} - u_\eta \frac{\partial \alpha}{\partial \tau}\right) . \tag{A18}$$

The Lagrangian surface motion is the same with

$$\frac{dz}{\partial t} = u \quad \text{and} \quad \frac{dr}{dt} = v \,. \tag{A19}$$

We take the no-slip boundary to be at some z=constant and require that

$$u_b = \left(\frac{\partial \phi}{\partial z}\right)_b + \left(\frac{1}{r}\,\frac{\partial \psi}{\partial r}\right)_b = \left(\frac{1}{r}\,\frac{\partial Q}{\partial r}\right)_b = 0 \,. \tag{A20}$$

Like with the rectangular case, we take the parts of the normal velocity to the solid surface to be individually zero, so that ψ like Q is constant on the solid boundary and the normal derivative of ϕ is zero.

With

$$v_b = \left(\frac{\partial \phi}{\partial r}\right)_b - \left(\frac{1}{r}\,\frac{\partial \psi}{\partial z}\right)_b = -\frac{1}{r}\,\frac{\partial Q}{\partial z} = 0 \,, \tag{A21}$$

we require

$$\left(\frac{1}{r}\,\frac{\partial \psi}{\partial z}\right)_b = \left(\frac{\partial \phi}{\partial r}\right)_b = (v_i)_b \,. \tag{A22}$$

Finally,

$$\omega_b = -\left(\frac{1}{r}\,\frac{\partial^2 Q}{\partial z^2}\right)_b = -\left(\frac{1}{r}\,\frac{\partial^2 \psi}{\partial z^2}\right)_b + \left(\frac{\partial v_i}{\partial z}\right)_b \,. \tag{A23}$$

TABLE I

t	ΔQ	Q_{max}	Q_{min}	$\Delta\phi$	ϕ_{max}	ϕ_{min}
$2.4 \cdot 10^{-3}$	$3.9 \cdot 10^{-3}$	$1.7 \cdot 10^{-2}$	$-1.7 \cdot 10^{-2}$	$9.8 \cdot 10^{-4}$	$6.4 \cdot 10^{-3}$	$1.7 \cdot 10^{-3}$
4.08	$1.95 \cdot 10^{-3}$	$9.2 \cdot 10^{-3}$	$-8.9 \cdot 10^{-3}$	$9.8 \cdot 10^{-4}$	0.0	$1.1 \cdot 10^{-2}$
12.0	$9.8 \cdot 10^{-4}$	$5.9 \cdot 10^{-3}$	$-5.7 \cdot 10^{-3}$	$9.8 \cdot 10^{-4}$	~0.0	$1.0 \cdot 10^{-2}$
26.7	$4.9 \cdot 10^{-4}$	$2.7 \cdot 10^{-3}$	$-2.4 \cdot 10^{-3}$	$4.9 \cdot 10^{-4}$	~0.0	$5.3 \cdot 10^{-3}$
40.7	$2.4 \cdot 10^{-4}$	$1.6 \cdot 10^{-3}$	$-1.4 \cdot 10^{-3}$	$2.4 \cdot 10^{-4}$	~0.0	$3.0 \cdot 10^{-3}$

TABLE II

t	ΔQ	Q_{max}	Q_{min}	$\Delta\phi$	ϕ_{max}	ϕ_{min}
0.09	1/128	$6.25 \cdot 10^{-2}$	~0.0	1/64	$1.47 \cdot 10^{-1}$	$-7.48 \cdot 10^{-3}$
0.92	1/128	$1.04 \cdot 10^{-1}$	0.0	1/32	$2.69 \cdot 10^{-1}$	$-2.35 \cdot 10^{-2}$
1.55	1/128	$1.13 \cdot 10^{-1}$	0.0	1/32	$2.80 \cdot 10^{-1}$	$-1.26 \cdot 10^{-1}$
2.80	1/64	$1.71 \cdot 10^{-1}$	0.0	1/16	$2.72 \cdot 10^{-1}$	$-4.76 \cdot 10^{-1}$
4.74	1/32	$2.79 \cdot 10^{-1}$	0.0	1/8	$4.56 \cdot 10^{-1}$	$-7.42 \cdot 10^{-1}$

REFERENCES

1. J. E. Fromm, "Finite Difference Computation of the Capillary Jet, Free Surface Problem," lecture notes in *Physics* **141**, 188-193, Seventh International Conference on Numerical Methods in Fluid Dynamics, Springer-Verlag, Berlin 1981.
2. J. E. Fromm, "A Numerical Study of Drop-on-Demand Ink Jets," Proceedings of the Second International Colloqium on Drops and Bubbles, NASA JPL Publication 82-7, California Institute of Technology, Pasadena (1982).
3. J. W. S. Rayleigh, *The Theory of Sound* Vol. 2, Dover, p. 351 (1945).
4. N. E. Kochin, I. A. Kibel, and N. V. Roze, "Theoretical Hydrodynamics," (Interscience Publishers John Wiley and Sons, Inc., New York 1964).
5. G. K. Batchelor, "An Introduction to Fluid Dynamics" (Cambridge University Press, Cambridge 1967).
6. J. Gazdag, Y. Takao, and J. Fromm, "Rigorous Numerical Treatment of the No-Slip Conditions in a Vorticity Formulation," Proceeding of the NASA Symposium on Numerical Boundary Condition Procedures, NASA Conference Publication 2201, Moffett Field, California, October 1981.
7. D. B. Bogy, J. E. Fromm, and F. E. Talke, "Exit Region Central Source Flow Between Closely Spaced Parallel Co-rotating Disks," *The Physics of Fluids* Vol. 20, No. 2, 176-186 (1977).

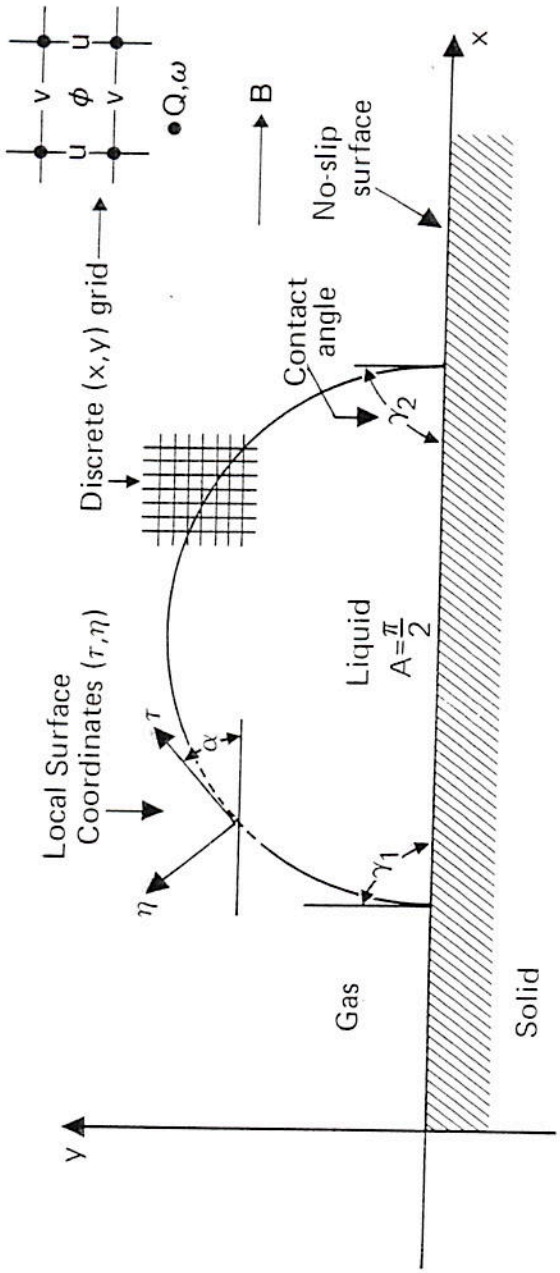

Figure 1. Geometry and scale.

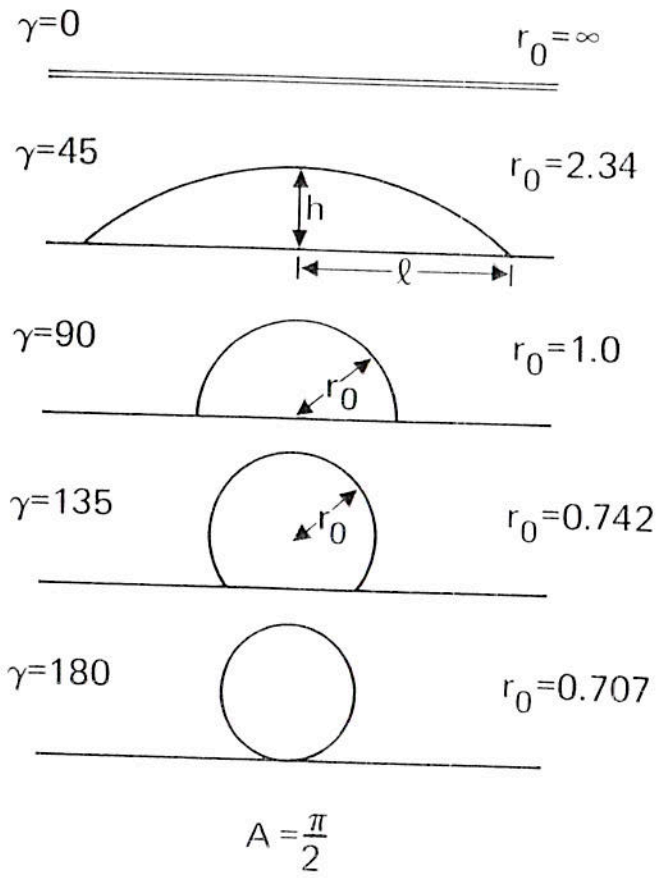

$$r_0^2 = \frac{\pi}{2\gamma - \sin 2\gamma}$$

$$h = r_0(1-\cos\gamma)$$

$$\ell = r_0 \sin\gamma$$

$$P \sim \frac{1}{r_0}$$

Figure 2. Equilibrium solutions for the rectangular case (constant cross-sectional area), B=0.

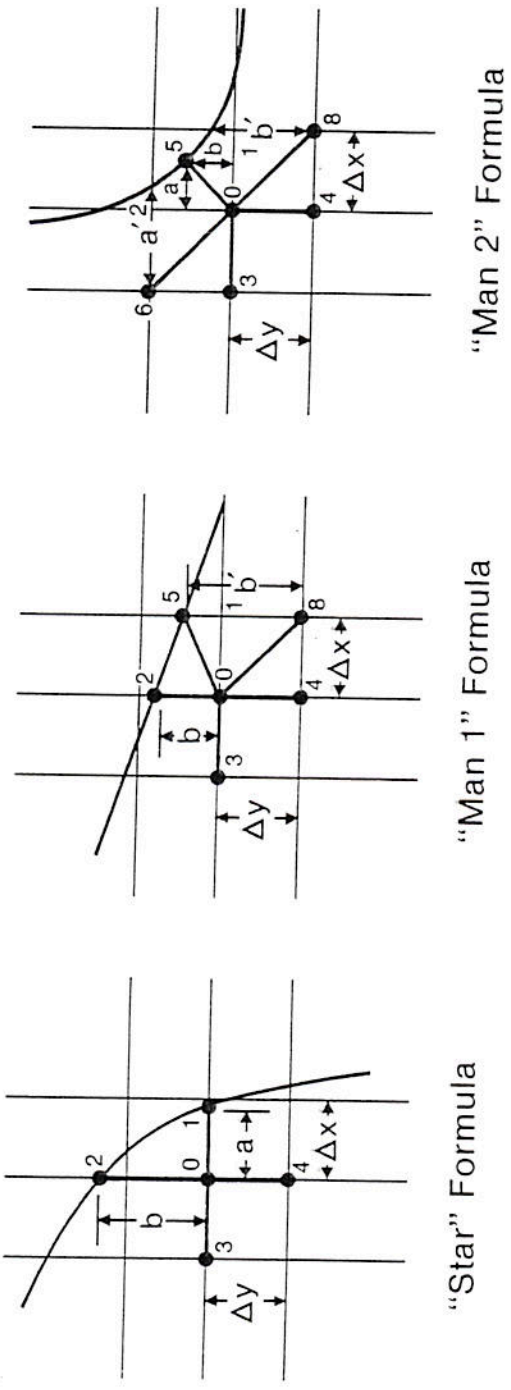

Figure 3. Grid layout for special near surface elliptic difference equation formulas.

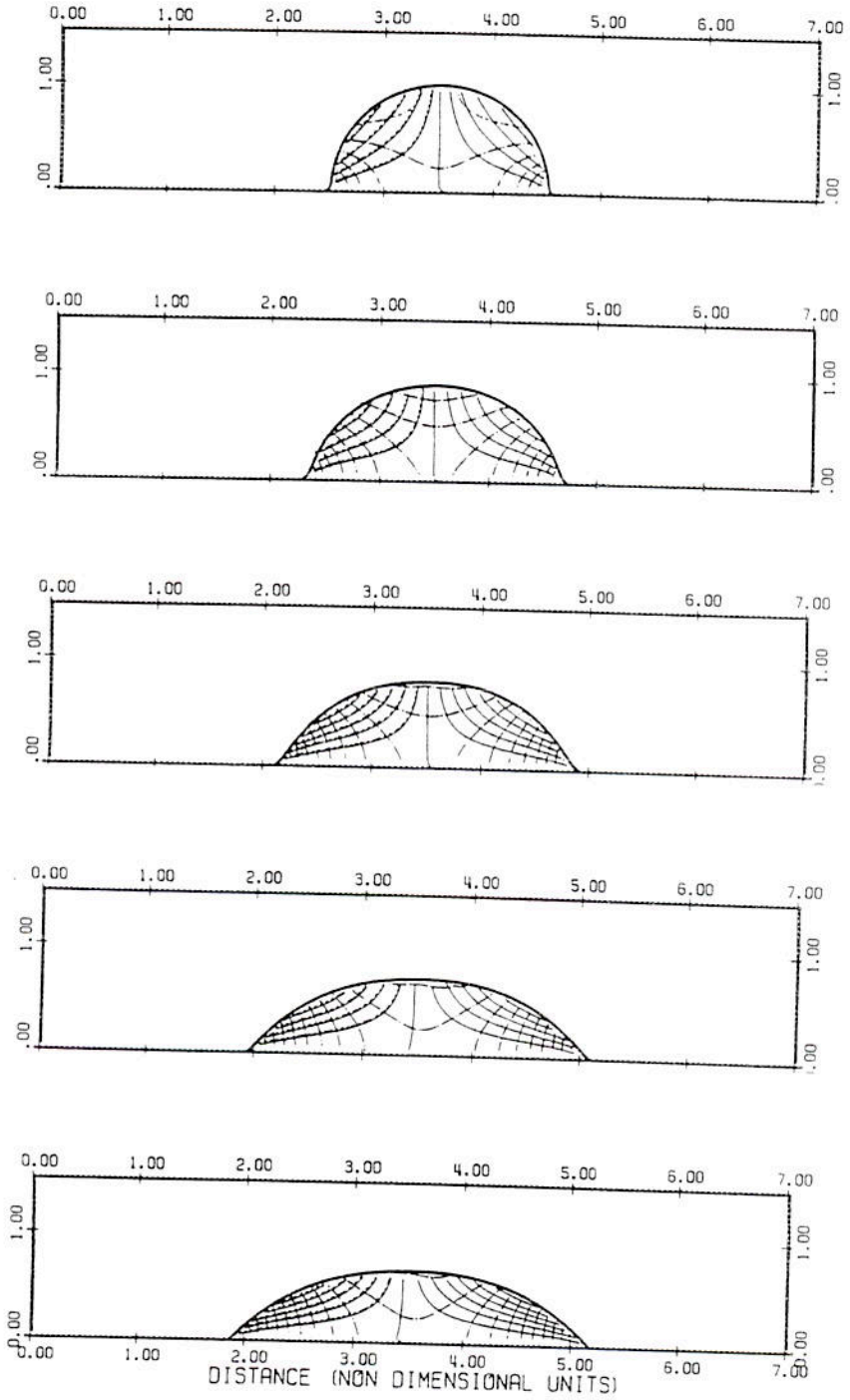

Figure 4. Time sequence of spreading for W/R=10, B=0, $\gamma_1=\gamma_2=45°$. See Table I.

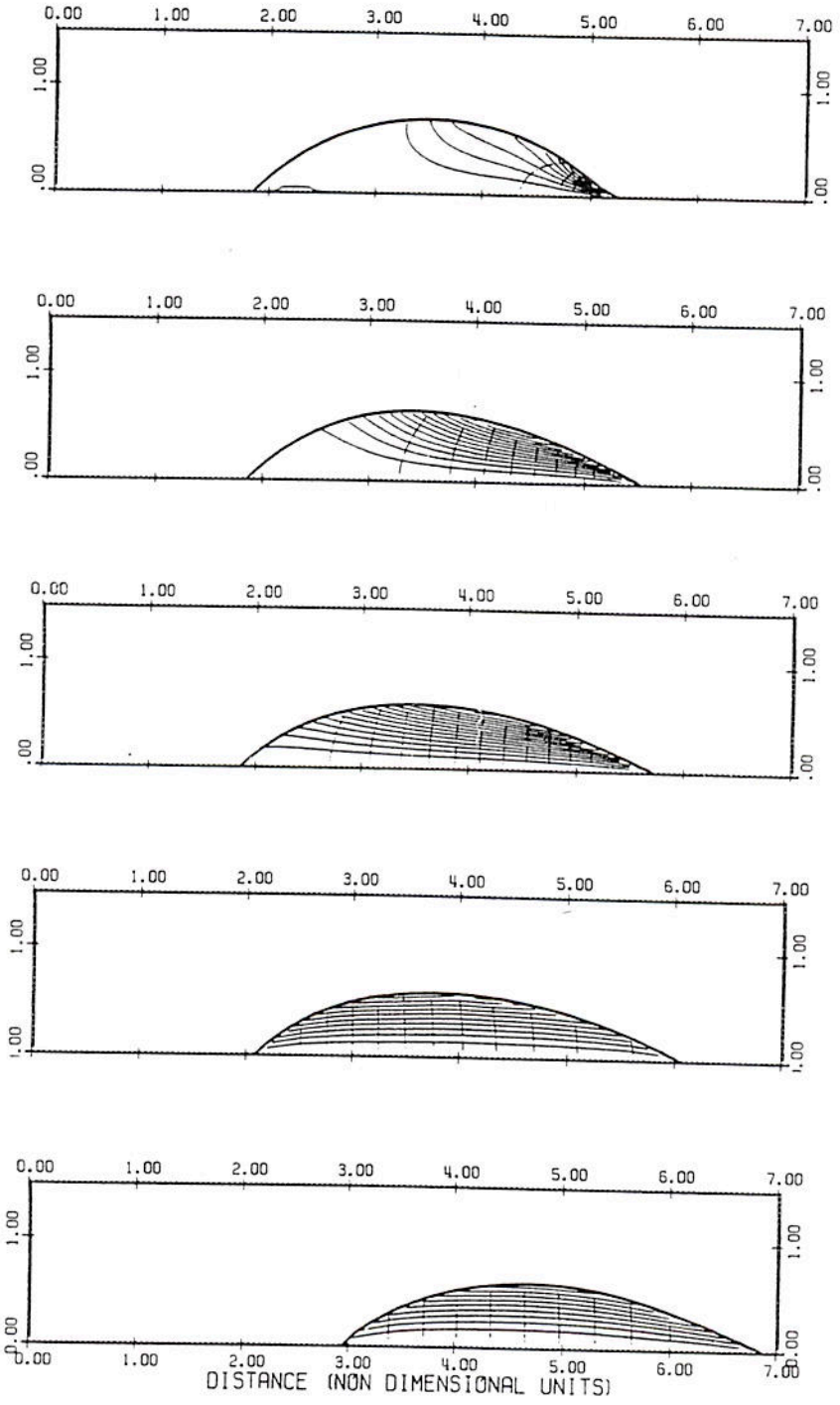

Figure 5. Time sequence of spreading into a higher surface energy region: W/R=0.05, B=0, γ_1=45°, γ_2=30°. See Table II.